Seasonal and diurnal patterns in the dispersion of SO$_2$ from Mt. Nyiragongo

Adam Dingwell[a], Anna Rutgersson[a], Björn Claremar[a], Santiago Arellano[b], Yalire Mapendano[c], Bo Galle[b]

[a]*Department of Earth Sciences, Uppsala University, Uppsala, Sweden.*
[b]*Department of Earth and Space Sciences, Chalmers University of Technology, Gothenburg, Sweden.*
[c]*Observatoire Volcanologique de Goma, Goma, Democratic Republic of Congo.*

Abstract

Mt. Nyiragongo is an active volcano located in the Democratic Republic of Congo, close to the border of Rwanda and about 15 km north of the city of Goma ($\sim$1,000,000 inhabitants). Gases emitted from Nyiragongo might pose a persistent hazard to local inhabitants and the environment. While both ground- and satellite-based observations of the emissions exist, prior to this study, no detailed analysis of the dispersion of the emissions have been made. We have conducted a dispersion study, using a modelling system to determine the geographical distribution of SO$_2$.

A combination of a meteorological model (WRF), a Lagrangian particle dispersion model (FLEXPART-WRF) and flux data based on DOAS measurements from the NOVAC-network is used. Since observations can only be made during the day, we use random sampling of fluxes and ensemble modelling to estimate night-time emissions.

Seasonal variations in the dispersion follows the migration of the Inter Tropical Convergence Zone. In June–August, the area with the highest surface concentrations is located to the northwest, and in December–February, to the southwest of the source. Diurnal variations in surface concentrations were determined by the development of the planetary boundary layer and the lake-/land breeze cycle around lake Kivu. Both processes contribute to low surface concentrations during the day and high concentrations during the night. However, the strong northerly trade winds in November–March weakened the lake breeze, contributing to higher daytime surface concentrations along the northern shore of Lake Kivu, including the city of Goma.

Sista stycket måste ändras:

Comparison between model result and reference values for SO$_2$, used as air quality regulation in the European Union (EU), is made. In Goma, the daily average concentrations exceeded the reference value ($125\mu g\ m^-3$) 120-210 days during a one-year period starting on the first of May 2010; the highest exposure was seen in the western parts of the city. These results indicate that as many as 1,000,000 people are exposed to potentially hazardous amounts of SO$_2$ from Nyiragongo.

Keywords: dispersion modelling, volcanic degassing, Nyiragongo, sulfur dioxide, FLEXPART-WRF

1. Introduction

Mt. Nyiragongo is an active stratovolcano in the East African Rift zone. It is located in the Democratic Republic of Congo (DRC), about 10 km west of the border to Rwanda and around 15 km north of the city of Goma, see Figure 1. Due to political instability in the region, people are moving away from the insecure country side to the city of Goma. The city currently has an estimated population of $\sim$1 million. It is therefore becoming increasingly important to study the natural hazards in the region.

Mt. Nyiragongo is unique by having the largest active lava lake in the world, it is one of the most important gas emitters on Earth. The ongoing humanitarian crisis prevents much needed risk reduction of future natural events, especially due to the close proximity to a large population. The situation also makes it difficult to carry out more extensive field studies; despite this, there have been some measurements of the source strength of SO$_2$ from Mt. Nyiragongo.

Mt. Nyiragongo's last eruption was in January 2002, when lava erupted on the southern flanks.

The lava flow passed through Goma and beyond the shore of Lake Kivu (Baxter et al., 2003), effectively dividing Goma in two. In totoal, 350 000 people were displaced, 120 000 were left homeless (Tedesco et al., 2007) and an estimated 70–100 fatalities resulted from accidents related to the lava flow (Komorowski et al., 2003).

Gases emitted by Nyiragongo pose a more persistent hazard to the surroundings. Monitoring of the emissions have been conducted as part of the global Network for Observation of Volcanic and Atmospheric Change (NOVAC) since 2007 (Galle et al., 2010). Several studies have been conducted in the region to assess the impact of gas emissions from Nyiragongo and the nearby volcano Nyamuragira. Methods applied to this region so far involve sampling of rainwater (*e.g.* Cuoco et al., 2013a,b) which found elevated concentrations of acidic halogens, SO_2^{2-} and NH_4^+ west of Nyiragongo. Calabrese et al. (2015) found elevated concentration of trace metals in rain water and vegetation samples in proximity of the crater rim, but decreasing with distance. In a field campaign carried out shortly after the eruption in 2002, Baxter et al. (2003) found no elevated concentrations of ground level concentrations of SO_2 in Goma in early 2002.

In this paper we present general patterns of volcanic gas dispersion under varying conditions. By combining observed gas fluxes with dispersion modelling we investigate whether elevated concentration of volcanic gases might occur in villages during certain conditions. The modelling approach allows for a quantitative analysis of ground level exposure.

This study is an important step towards bridging the knowledge of emissions with observed impact by providing results from dispersion modelling of measured emissions from Mt. Nyiragongo.

2. Health effect of SO_2

Ta bort stycke+tabell?

The World Health Organization (WHO) have presented guidelines for maximum average concentrations of SO_2 over different time periods. These guidelines are for simplicity suggested regardless of environmental condition or presence of particulates which may both influence the health effects (WHO, 2006). Some of the guidelines have been implemented in legislation by e.g. the European Union. A summary of these guidelines/restrictions (from the WHO and the EU) is presented in Table 1. In this study, we have used the EU's air quality standards for 24-hour averages, and 1-hour averages as reference values. Exceeding the 24-hour reference value over longer periods can be connected to increased mortality rates (WHO, 2006) while short term exposure above the 1-hour values is used as an indicator for acute health impact.

Lägg till kommentar om gränsvärdenas betydelse om stycket behålls.

3. Method

3.1. Meteorological data

Reanalysis data was used as the initial meteorological data. Reanalysis data is an integration of all available observations into a modelling system, for the the best possible description of the state of the atmosphere. Meteorological data at a resolution of 0.75°, from the reanalysis product ERA-Interim (Dee et al., 2011) was used to force the Weather Research and Forecasting (WRF) model. WRF is a 3-dimensional, non-hydrostatic mesoscale model, frequently used for a variety of applications (e.g. Rögnvaldsson et al., 2008; Pohl et al., 2011; Steensen et al., 2013).

For this study, WRF was set up to downscale in 4 steps from 72 km to 2 km resolution. Most surface data is available at ∼1 km resolution so there is little benefit from using higher resolutions. The vertical resolution was set to 60 levels, with the lowest level spanning approximately 0–60 m a.g.l. The innermost domain was set to cover an area of 350×300 km, as shown in Figure 1.

The simulations used the WSM5 microphysics scheme by Hong et al. (2004), , the Noah land surface model (Tewari et al., 2004) and the Janjić (1994) surface layer physicsthe and boundary layer schemes. The outer domains also used the Kain (2004) convection scheme.

The WRF model was run in 60-hour segments, were 12 hours were used for spin-up followed by 48 hours for the main production of results. Initial tests showed that a shorter spin-up period was not sufficient for our configuration. Soil layers were spun up over a longer period, based on the method described by Angevine et al. (2014). More specifically, the model was run for a month to initialize soil moisture and temperature. At the end of each spin-up segment, soil data from the end of the previous production segment were copied over to be used in the new production segment. In a similar
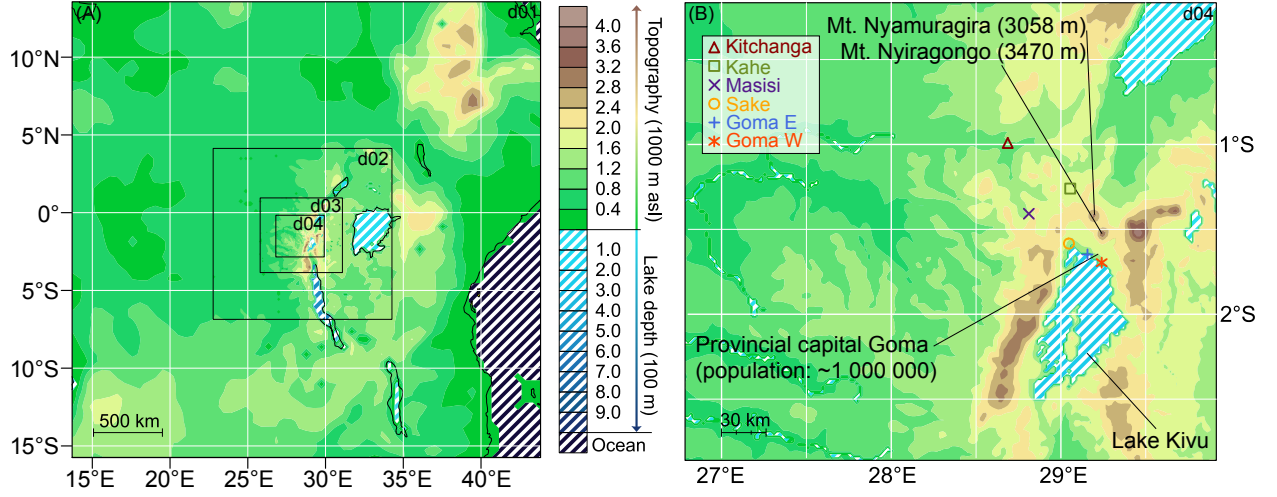
Figure 1: Topographic maps over the region of study as interpreted by the meteorological model, (A) shows all nested domains (1-4) used for downscaling, (B) shows the innermost domain (4). The main dispersion simulations in this study only use data from the innermost domain. Also shown in (B) are the locations of a number locations covered in more detail by this paper.

Table 1: A summary of air quality guidelines from the World Health Organisation (WHO) and air quality standards set by the European Union (EU) in 2005. The values apply to SO_2 concentrations averaged over intervals from 10 minutes to 24 hours.

SO2-concentration $\mu g\ m^{-3}$	averaging interval	Comment
500	10 min	WHO (2006)
350	1 hour	EU standard since 2005
125	24 hours	WHO (2000), EU standard since 2005
20	24 hours	WHO (2006)

3

fashion, accumulated fields, such as precipitation, were also inherited at the end of each spin-up period to produce consistent, increasing fields. Consistently increasing precipitation is a requirement for the dispersion model.

3.2. Emission data

Four stations have been deployed at distances between 10 and 15 km SW from the summit of Nyiragongo volcano to monitor SO_2 emissions since March 2004. These stations are now integrated into the NOVAC network (Galle et al., 2010). Each site consists of a scanning remote sensing instrument and telemetry for real-time data transmission to the Goma Volcanological Observatory. The measurement strategy consists in acquiring UV spectra (280–420 nm) from the sky over a flat or conical cross section surrounding the volcano. From each spectrum the column density of SO_2 is derived based on the DOAS (Differential Optical Absorption Spectroscopy) (Platt & Stutz, 2008) technique. The integral of column densities over the scanning plane, which depends on plume direction and height, is multiplied by the wind speed at the centre of mass of the plume to obtain the emission rate of SO_2. When more than one station locates the plume at about the same time, it is possible to derive the plume direction and height by triangulation, otherwise this information has to be provided by other means. The temporal resolution of the measurements is of the order of 5–10 min, depending on the amount of UV-radiation. The uncertainty of each measurement is about 35–50%, depending mostly on uncertainties in plume speed and radiative transfer effects. Technical details of the instruments and the retrieval method can be found elsewhere (e.g. Galle et al., 2010; Arellano, 2014).

For the period of time of this study, unfortunately only one station provided valid measurements (Rusayo station located at 1.57699°S, 29.1799°E, 1693 m a.s.l., azimuth 90 deg, conical scanner). Plume direction, height and speed were obtained by combining the information on the scan angle where the centre of mass of the plume was found, with vertical profiles of wind speed obtained from meteorological modelling. The algorithm looks for the altitudes at which the modelled winds can explain the observed angular position of the plume. The closest to ground of such altitudes is assumed to be the plume altitude; the corresponding wind speed and direction is then used for the respective flux measurement. If the algorithm cannot find correspondence between modelled and observed plume directions the plume is assumed to be at summit altitude (3470 m a.s.l.). Fluxes and plume altitudes calculated using this method are presented in Figure 2.

Since observations can only be made during the day in fairly clear weather, there are both regular (nightly) and irregular gaps (e.g. due to bad weather, technical and/or security issues) in the time series. When simulating the dispersion, it typically takes several days for particles to travel across the domain, depending on altitude and meteorological conditions. The dispersion model must therefore run over several observation gaps before it is properly spun-up.

It is necessary to fill the gaps in the observations in order to produce useful results with the model. We do this by random sampling of observations within the period of study (i.e. April 2010 – April 2011) when a gap longer than 60 minutes is encountered. Each gap will be filled by a number of samples equal to $t_{gap}/t_{segment}$ rounded up to the nearest integer, where t_{gap} is the duration of the gap and $t_{segment} = 30\,\mathrm{min}$ is the default duration during which a sample will be used.

The segment duration of 30 min was chosen in order to be able to resolve the typical puffs otherwise seen in the observations. A shorter sampling interval will result in puffs being cut off, reducing their impact on the down wind concentrations. A longer interval will, however, have the opposite effect resulting in a higher influence from each sample.

In order to estimate the error of this method, the above sampling technique was applied to create 30 different time series of fluxes, covering the same period. A dispersion simulation was set up for each of the generated time series, forming an ensemble of 30 members.

3.3. Atmospheric dispersion model

The Lagrangian Particle Dispersion Model FLEXPART-WRF (Brioude et al., 2013) was used to simulate the transport and deposition of SO_2. FLEXPART-WRF has previously been used for a variety of applications. Srinivas et al. (2014) estimated radiation risk following the 2011 Fukushima nuclear accident using FLEXPART-WRF, the model was able to reproduce observed deposited activity with some deviations related to modelling errors in wind and precipitation data
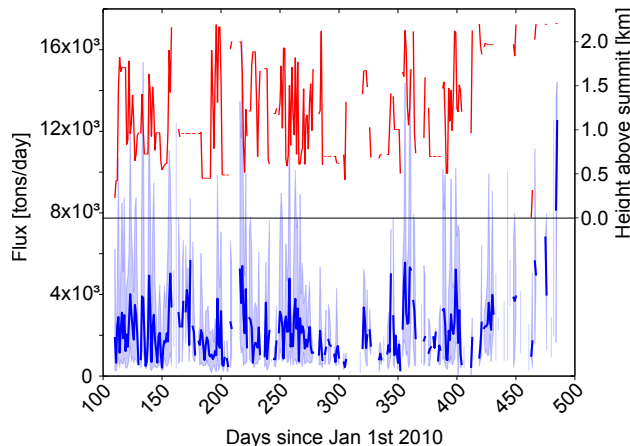
Figure 2: Daily averaged SO$_2$ fluxes based on the DOAS observations (see text for details). The bold (blue) line shows the average SO$_2$ flux, the shaded (blue) area shows the daily minimum and maximum fluxes. The narrow (red) line shows the daily average plume height estimated by matching wind direction and the observed plume alignment.

from WRF. Gentner et al. (2014) used FLEXPART-WRF in backward mode for determining source footprints of anthropogenic emissions of organic carbon; the footprints were consistent with results from aircraft observations. Another recent study where backward mode was used was made by Liu et al. (2015), where FLEXPART-WRF was used to determine the contribution of black carbon from the northern hemisphere to the European Arctic. The FLEXPART-WRF simulations were consistent with corresponding back-trajectories from HYS-PLIT. Dingwell & Rutgersson (2014) studied the long range dispersion of volcanic ash from a number of eruption scenarios on Iceland. The study presented in this paper uses a similar method as used by Dingwell & Rutgersson (2014), but also incorporates measurements of the near-source emissions.

For this study, two sets of simulations were conducted. First, a single model run was made, starting on the 1st of April 2010 and covering one year. Emissions from Nyiragongo were represented by a volume source with a base square of 1x1 km, centred around 1.5219°S, 29.249°E, and extending from the surface up to 4 km above ground level. The source strength was fixed at 10 kg/s.

The second set was an ensemble of 30 simulations (members), starting in mid-April, based on flux data from the NOVAC database. Each member used the observed fluxes when available and generated its own set of emissions according to the sampling method described Section 3.2. The top of the source volume was determined by the plume height estimates. The scatter of the ensemble members was used to estimate the uncertainty of the method.

All simulations had a release rate of 1000 computational particles per hour. The particles were set to split at the age of 6 hours to improve accuracy at longer distances from the source. Concentrations were sampled on a 3-dimensional output-grid every 3 minutes and used to calculate hourly averages. The horizontal resolution of the output-grid was set to match the meteorological model (2x2 km). The ensembles used a variable vertical grid spacing starting at 25 m at ground level and decreasing by altitude. A high resolution near the surface was important since surface concentrations were the main focus. The output grid is only used at the output stage of the FLEXPART-WRF or when determining if a particle has left the model domain. Therefore, it was unnecessary to retain the high vertical resolution at higher levels, where no detailed analysis of the data would be performed.

The fixed-source simulation used a uniform vertical grid spacing of 500 m. This was chosen since the results where used to study the vertical distribution of the emissions, which is best made using a uniform grid. Both sets assigned the top level of the model grid to 25,000 m a.g.l. to prevent any particle loss at the top of the grid.

3.4. Modifications to the dispersion model

Early on in this study, we encountered problems with the land-use data in FLEXPART-WRF. The model was using the same land-use data base as

5

the parent model, FLEXPART; the land-use data base has a resolution of 0.3 degrees. When running at higher resolutions, in our case with 2 km meteorological data, dry deposition data showed clear artifacts from the land-use grid. For an improved land-use description, FLEXPART-WRF was modified to optionally read land-use data from the WRF model. With new input routines, dry deposition becomes more realistic with land-use and meteorological data on the same resolution. Results from simulations using the different land-use data sets are shown in Figure 3.

Figure 3A shows one year accumulated dry deposition from the new land-use data divided by the old data. The difference in resolution is clearly visible. Locally, the two data sets deviate up to a factor 4 from each other (in either direction). The area around the NW tip of lake Kivu, shows a strong difference between the land-use modules. This area is directly downwind of the source most of the year. Therefore, it has a strong influence of surface concentrations, this is demonstrated in Figure 3B, where average surface concentrations for September–November 2010 are compared. Using the new land-use data results in 5-20% higher surface concentrations over the studied region, compared to when using the old data. A more detailed description of the new land-use routines is given in Appendix A.

4. Results using a uniform source

Results from the constant source simulation were used to study seasonal and diurnal variation of the dispersion originating from meteorological factors.

4.1. Seasonality

Figure 4 shows seasonal averages of the vertically integrated plume, covering the period from April 2010 to March 2011. June–August (Fig. 4C) showed the strongest meridional transport of the studied periods. The simulations show that the plume covered most areas around Lake Kivu frequently during this period. Another portion of the emissions were transported to the north, with pollutants reaching further north than any other time of the year. The southward transport over lake Kivu was also visible for December–February, however, in this case more affected by topography.

In contrast, the periods covering the equinoxes (September–November and March-May) show the strongest westward transport. During these periods, the ITCZ passes over the region, resulting in strong easterly winds.

A cross-section of the plume was extracted along the marked line in Figure 4. The cross-sections are shown in Figure 5. There is a clear seasonal shift in the skewness of the plume. In December–February the main portion of the southward transport occurs near the surface. At higher altitudes, the meridional transport becomes northward. In June–August, when the meridional transport was most efficient, the above pattern was reversed; northward transport was dominated by lower portions of the plume while southward transport was predominant at higher altitudes. The remaining two periods (March–May and September–November) showed less skewness.

The seasonal variation in plume alignment corresponds well with the migration of the ITCZ. In June–August, surface winds have a stronger southerly component since the ITCZ has shifted to the north. At higher altitudes the winds turn somewhat to have northerly component instead. In December–February the pattern reverses. Over the transition periods (September-November and March-April) there is less difference in wind direction between different altitudes.

4.2. Diurnal variation

Diurnal variations of concentrations along the cross section (Fig. 4) and their dependency on season is shown in Figure 5. The highest ground level concentrations, at this distance from Nyiragongo, are usually found near the north bank of Lake Kivu (1.6°S), just before sunrise (∼06:00 local time). During the day, concentrations generally decrease near the surface, but increase at higher altitudes. During the night, a thin layer with high SO_2 content is seen extending out over the surface of Lake Kivu. These high surface concentrations are most pronounced in November–February. In June–August, this diurnal variation is weaker; the area with the highest exposure is instead on the northern slope (north of 1.4°S).

Diurnal variations in the dispersion are partially explained by the depth of the boundary layer, as a deeper layer usually results in lower concentrations near the surface. The high concentrations seen near the northern shore of Lake Kivu, and their diurnal variation, correspond with expected behaviour of lake-/land-breeze circulation and katabatic/anabatic winds. In midday, when insolation
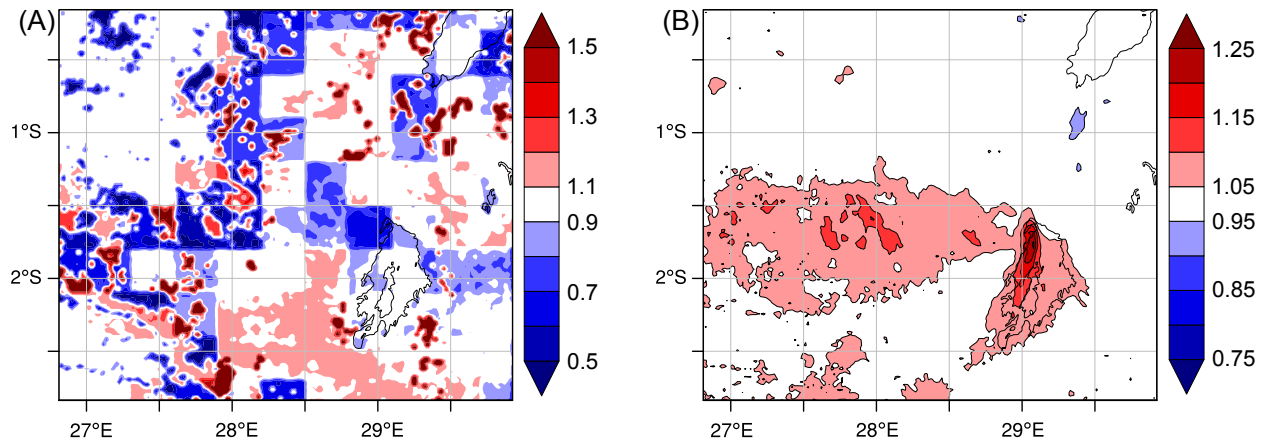
6

Figure 3: Relative difference between results from different land-use modules in the dispersion model; these were calculated by dividing results from the new module with those from the old. (A) shows the relative difference in dry deposition after one year of simulations (April 2010 – March 2011). (B) shows the relative difference in average concentrations within 500 m of the surface , covering the period September–November 2010.
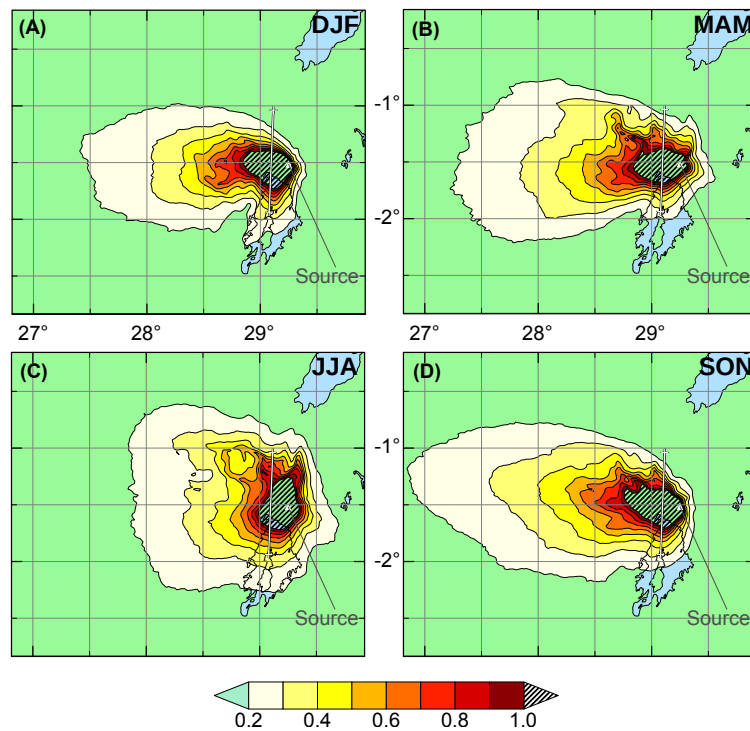

Figure 4: Modelled seasonal averages of the vertically integrated SO2 column, given in Dobson Units. The data covers one year from April 2010 to March 2011 and uses a constant emission source. The position of the emission source (Mt. Nyiragongo) is marked with a white triangle. The black and white line marks a cross section of the plume.
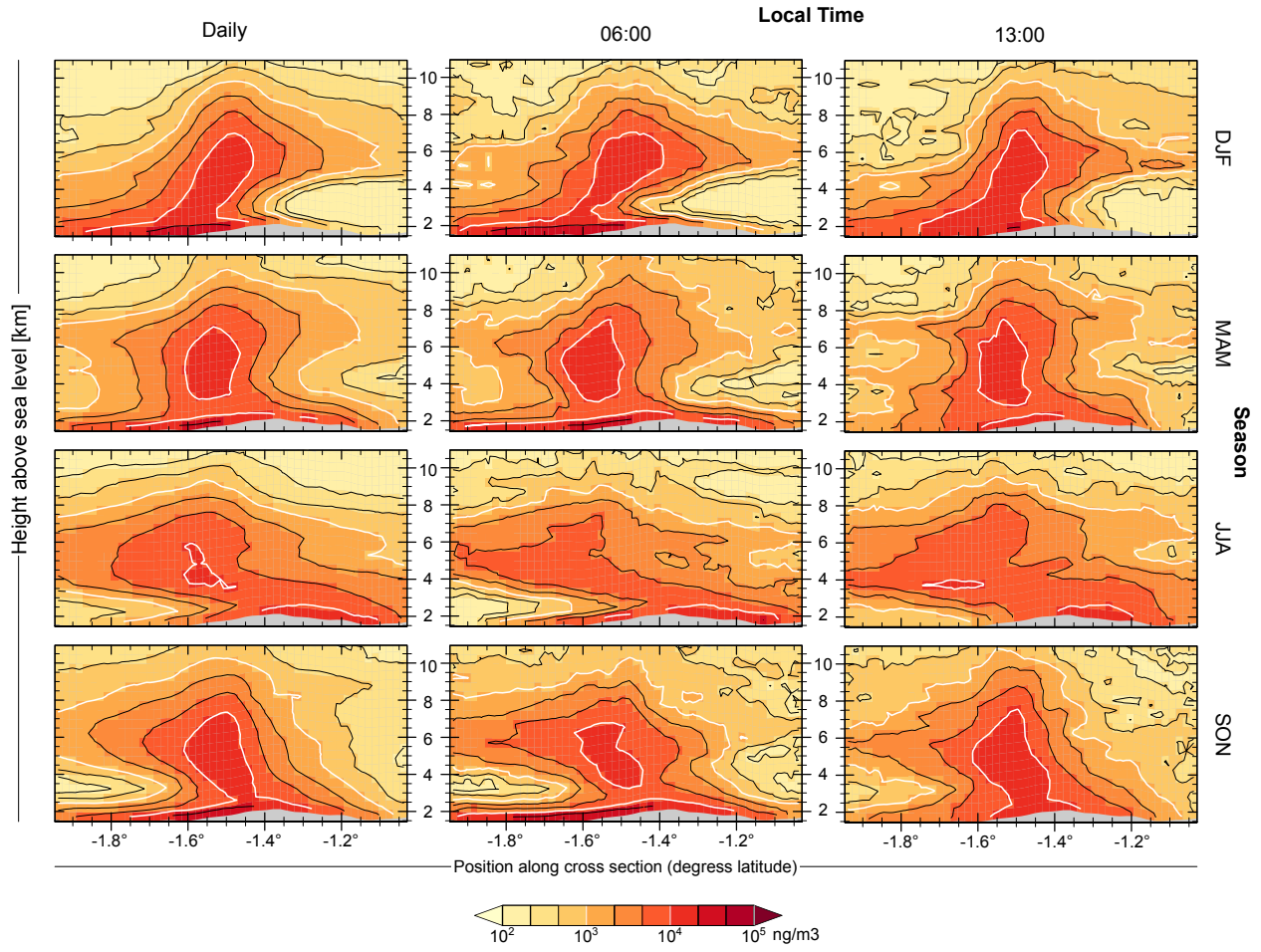
Figure 5: Modelled seasonal average diurnal variation of SO2 along the cross section marked in Figure 4. The leftmost column shows average concentrations for each 3-month period. The middle column show average concentrations between 05:00–06:00, local time (i.e. just before sunrise), the rightmost columns shows average concentrations between 12:00–13:00 (i.e. first hour after maximum insolation). The two leftmost columns represent the diurnal extremes, regarding the concentrations over Lake Kivu. The data covers one year from April 2010 to March 2011 and uses a constant emission source.

is strong, the slopes north of lake Kivu are well suited to develop anabatic southerly winds. Together with the lake, a lake-breeze is likely to form, also with southerly winds at the surface. These two effects result in lower surface concentrations near the coast-line during the day.

After sunset, the lake-breeze and anabatic winds weaken and eventually a reverse system forms. This system is at its strongest when the temperature difference is largest – just before sunrise. This results in the formation of a shallow layer with a high SO_2-content, stretching from the slopes north of Lake Kivu and as far south as Idjwi island (1.93°S).

5. Results from source based on observed fluxes

We now consider the cases where observed fluxes were used to determine the emission strength and altitude. The results represent our best estimate of SO_2-concentrations over the region for the period April 2010 to March 2011.

Figure 6 shows the number of times hourly averaged concentration of SO_2 exceeded different reference values. This type of figure was chosen since the concentration at a specific site is either at the background level (i.e. 0 in the raw model output) or follows a log-normal distribution. Therefore, presenting averages of the entire time series for a given location will only be misleading. Different trends are seen in the southern sites (Figure 6A-C) compared to the northwestern sites (Figure 6D-F). In Sake (A) and Goma (B,C), the highest exposure was reached in October 2010 – March 2011. The SO_2-concentrations in these areas stayed below, or near, background concentrations most (∼80 %) of the time in April–August 2010.

In Kahe and Kitchanga (Figure 6D-E, the pattern was nearly reversed, with the lowest concentrations seen in November 2010 through March 2011, and the highest in April through September 2010. Masisi, being located further south, had a weaker seasonal variation.

In September the conditions changed, concentrations in communities WNW of Nyiragongo (Ksebere and Masisi) increased as the southerly winds weakened. An increase was also seen in Sake and Goma (especially the western parts). In October, the plume had shifted far enough south to allow cleaner air in both Kahe and Burungu. Instead, areas around lake Kivu were exposed. In November,

Masisi reached its highest exposure in 2010, exceeding 100 $\mu g\ m^{-3}$ 30 % of the time with occasional periods above 1000 $\mu g\ m^{-3}$. At the same time, exposure to SO_2 in Sake and Goma was increasing. The maximum exposure in Goma and Sake was reached in January–February 2011; during this period, western Goma exceeded 1000 $\mu g\ m^{-3}$ 20 % of the time.

Depending on season, different patterns are also expected over the diurnal cycle. Diurnal variations in SO2-concentration for different months are shown in Figure 7. Surface concentrations were typically lower during the day for all communities throughout the year, as is expected from a convective boundary layer; in daytime, hourly average concentrations above 1000 $\mu g\ m^{-3}$ were rare.

The same seasonal variation was seen as for the unsorted averages in Figure 6, however, the diurnal variation differed somewhat between locations. In July 2010, when the average dispersion direction at the surface was aligned to the WNW, the exposed communities had a strong diurnal variation in SO_2-concentrations. Nighttime concentrations in Kahe were above 1000 $\mu g\ m^{-3}$ 20 % of the time, while daytime concentrations were mostly below.

In November–March, when the southern communities reached their maximum exposure, diurnal variations were weaker. This is largely due to the ITCZ being shifted to the south, causing northerly surface winds over the region. The northerly winds were strong enough to prevent the lake-breeze at the northern shore of lake Kivu from fully developing. Instead, emissions were transported southwards, past the shoreline.

Furthermore, In April–July there was an increase in cases with elevated trace amounts of SO_2 (concentrations above 10 $\mu g\ m^{-3}$) during the day, while higher concentrations were only seen during the night. Masisi is located on the western foothills of the Virunga mountains so pollutants need to be transported downward after passing a mountain range. This can occur as increased downward mixing over the valley during the day or as downhill winds along the slopes during the night.

6. Discussion

Throughout all simulations we assume that SO_2 will be released from the surface and up to the matched plume height. This might result in higher concentrations near the surface further downwind, compared to if an elevated plume is assigned; this
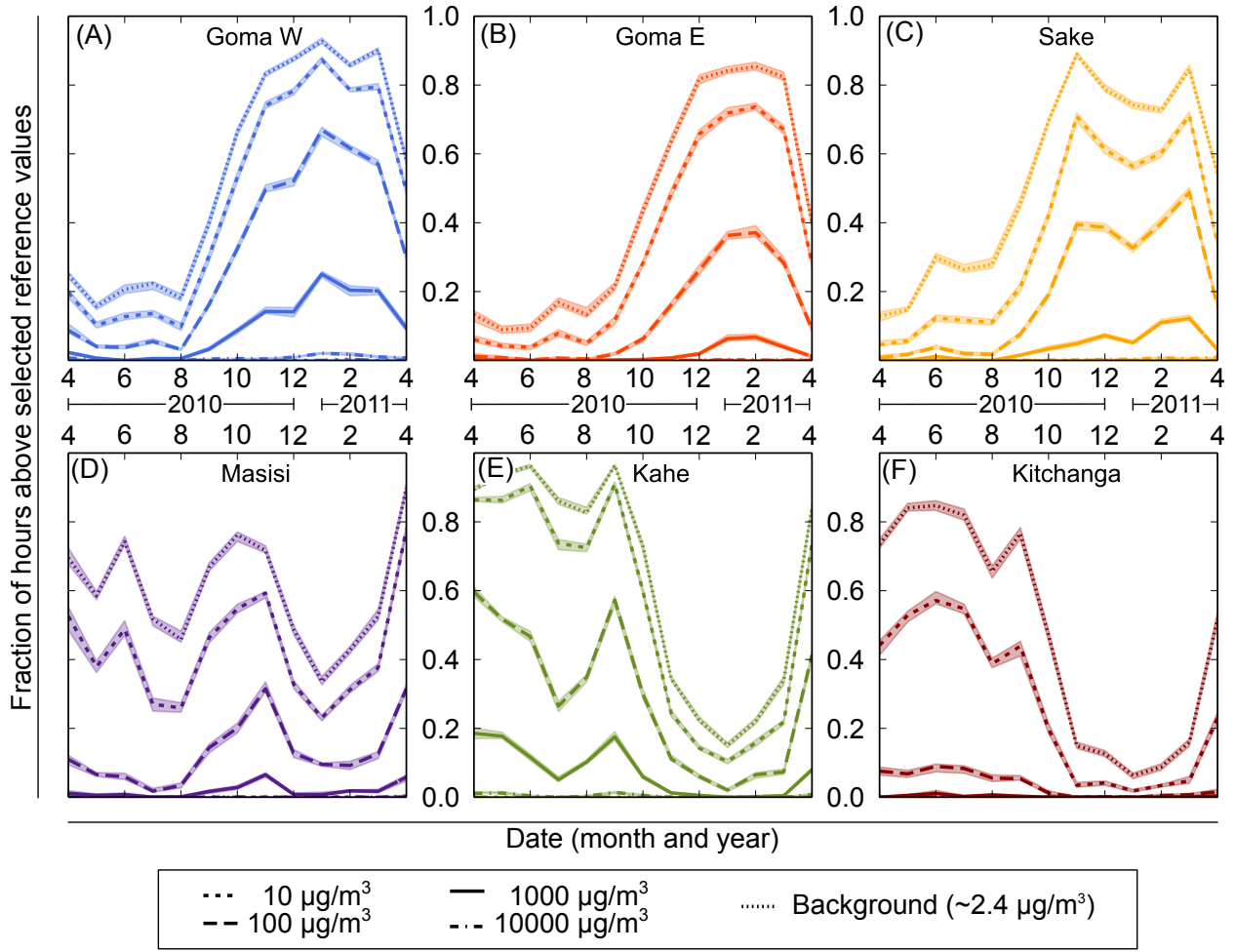
Figure 6: Fraction of hours with concentrations exceeding different thresholds, displayed for a selection of populated (A-F) marked in Figure 1B. The lines represent the median of 30 scenarios and the shaded areas show the 10- and 90-percentiles. The lowest threshold corresponds to corresponds to clean continental background concentrations, i.e. when the sites were not directly influenced by the modelled plume.
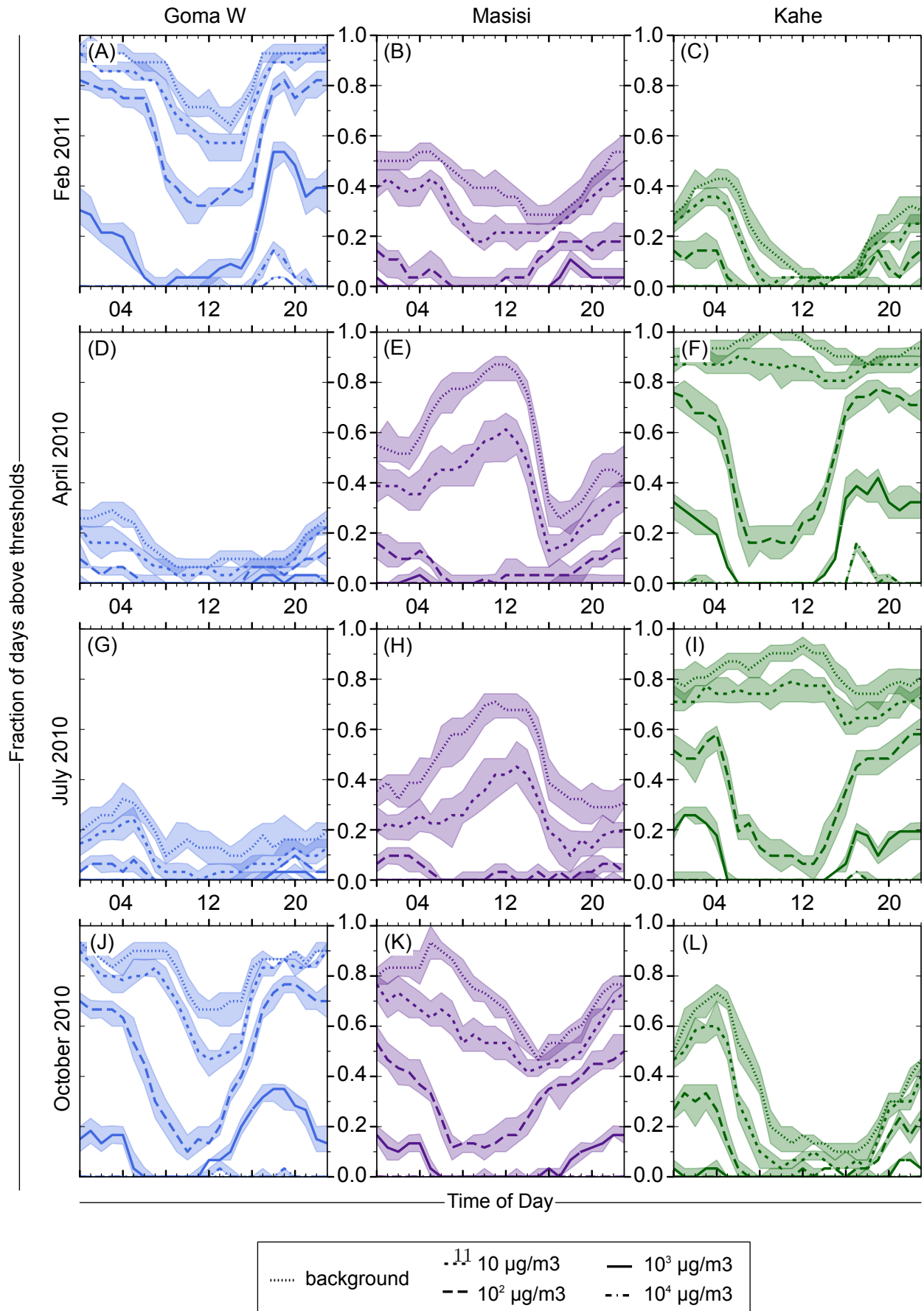
Figure 7: Fraction of days with hourly average SO2-concentration above different thresholds (as indicated by different dash-patterns). Three different locations are presented (left to right): western Goma, Masisi and Kahe (see Figure 1B). The lines represent median number of total exceedances of the different thresholds, the shaded areas represent the 10-90 percentile exceedances. An ensemble of 30 members was used to produce these results.

is mainly relevant when the boundary layer is less stable (e.g. during the day). Furthermore, less mass is released at higher altitudes resulting in lower concentrations where the main plume was observed. An alternative method would be to adjust the plume centre to match the observed height; the problem with such a method is to estimate the vertical span of the source volume. There are no observations of the plume thickness, and therefore, further assumptions need to be made in order to assign a variable source depth.

The ensemble method used in the dispersion simulation should account for part of the error introduced by sampling flux data to fill gaps in the time series. However, the method does not account for long term trends in the emissions or the measurement error. Such trends could be incorporated by assigning a higher probability to observations closer in time relative to the gap in question.

We see no clear correlation between plume rise and emission strength; this suggests that atmospheric conditions have an important influence. This study makes no attempt at including atmospheric influence on plume rise. Since observations are only made in daylight, there might be a systematic overestimation of the plume rise during the night. A overestimated plume rise might result in lower surface concentrations, especially during the night (when there is less turbulent mixing).

This study only covers sulphur in the form of SO_2. In FLEXPART-WRF SO_2 is removed from the atmosphere solely through dry deposition; chemical reactions are not supported. Over short time spans this is usually a reasonable assumption, however, volcanic plumes are chemically very active. Radke et al. (1976) found significant particle formation in effusive plumes within several kilometres of the vent. Later studies have found sulphate aerosols in volcanic plumes close to the vent, either formed through rapid gas-to-particle formation or emitted directly as primary particles (Allen et al., 2002; Mather et al., 2003; Allen et al., 2006). Furthermore, dissolved sulphate from Nyiragongo has been found in rainwater collected at or near the vent (Cuoco et al., 2013a). Whether this is due to direct emissions of sulphate particles or due to rapid oxidation of SO_2 is not known, however, it is not included in our simulations. Therefore the model is systematically overestimating the SO_2-concentration. However, several sources of uncertainty in SO_2 flux measurements tend to produce underestimation of the source emission; this under-

estimation is mostly due to the effect of radiative transfer at large distances from the plume, and the removal of SO_2 between the source and the observed cross section.

We made one test to study the importance of wet removal of sulphates downwind from the observations by creating a modified model particle with the same properties as SO_2 but with wet scavenging coefficients set to match the built-in sulphate aerosols in FLEXPART-WRF. The removal rate of this particle should represent the fastest possible removal rate of sulphur from the atmosphere. The largest difference between the default and modified SO_2 is seen in September–November (2010). This period covers the peak of the rainy season; the enhanced removal through washout results in 20–30 % lower surface concentrations when using the modified particles. However,The smallest difference between the two particle types, is seen in March–May, not during the dry season (i.e. June–August). This happens because the westward transport is more efficient in March–May than in June–August, reducing the probability of the plume being washed out close to the source.

Deep convection is also a factor, our model system can theoretically resolve such events, but no attempt has been made to verify if convection cells occur at the correct times and locations.

An earlier study by Sawyer et al. (2008), determined the main constituents of the emissions from Mt.Nyiragongo and their proportions. Since little variation was found in the mixture over time, this information could be used to extend this study to cover other substances as well. However, most of these substances are not currently included in the dispersion model, i.e. there are no wet- or dry scavenging coefficients for them.

7. Conclusions

We have shown how the dispersion of SO_2 from Nyiragongo changed over the period April 2010 to April 2011. The seasonal variations of the dispersion agree well with the migration of the ITCZ, seen as vertically skewed plumes around the solstices and more uniform plumes around the equinoxes. Similar results are expected for following years.

A diurnal variation in the dispersion is linked to land–lake breeze circulation, possibly enhanced by katabatic/anabatic winds and channel flow. The diurnal variation will transport low altitude emissions southward, out over lake Kivu, during the night.

Areas south-west of Nyiragongo, including Goma, are most likely to be exposed to emissions during the night and early morning. Between November 2010 and March 2011, strong northerly trade winds frequently prevented the lake breeze from fully forming around the northern shore of lake Kivu. During this period hourly average SO_2-concentrations in Sake and western Goma exceeded 1000 $\mu g\ m^{-3}$ on several occasions during daytime (5–10 % of the time). Suggesting that there might be periods of increased exposure to volcanic gases in these areas. This stresses the need for a longer measurement campaign in order to reliably map the the exposure to emissions from Mt. Nyiragongo.

Acknowledgements

Appendix A. New land-use module in FLEXPART-WRF

As part of this study, a new method for assigning land-use in FLEXPART-WRF had to be implemented. The new method will read land-use data from WRF while the original method would use a compressed data file supplied with the model. The original method for assigning land-use was left unmodified, so the user can chose which method to use at run-time. The method is chosen by setting LU_OPTION to 1 for WRF or 0 for the original data.

No changes were made in how land-use is stored in memory or how it is later interpreted by the dry deposition scheme. A description of the land-use implementation in FLEXPART V8.2, which is also valid for FLEXPART-WRF, can be found in the user guide (available at `www.flexpart.eu/downloads`). In short, FLEXPART-WRF will assign surface area fractions of the three most common land-use categories in each grid cell. When using the new method, FLEXPART-WRF will usually only assign one land-use category per grid cell, since this is how WRF stores land-use data. There are exception, *e.g.* "Mixed Tundra" in WRF will be assigned as 50 % each of "Mixed Forest including Wetland" and "Barren land, mostly desert" in FLEXPART-WRF.

Table A.1 shows how FLEXPART-WRF interprets MODIS data from the WRF model. This interpretation is almost the same as in the original FLEXPART code, with the exception that WRF supplies three additional classes for different types of tundra.

Table A.2 shows how FLEXPART-WRF interprets USGS land-use data from the WRF model. This table is mainly based on the corresponding table used by WRF-CHEM, with some modifications to better suit the implementation in FLEXPART. For comparison, the corresponding land-use classes used for dry deposition in WRF-CHEM are also given.

Table A.1: MODIS WRF to FLEXPART-WRF converstion table (same table as is already used in FLEXPART and its derivatives)

	MODIS − WRF		Wesely − FLEXPART-WRF
1	Evergreen Needleleaf Forest	5	Coniferous
2	Evergreen Broadleaf Forest	13	Rainforest
3	Deciduous Needleleaf	4	Deciduous Forest
4	Deciduous Broadleaf Forest	4	Deciduous Forest
5	Mixed Forest	6	Mixed Forest including Wetland
6	Closed Shrublands	11	rocky open areas with growing shrubs
7	Open Shrublands	11	rocky open areas with growing shrubs
8	Woody Savannas	11	rocky open areas with growing shrubs
9	Savannas	11	rocky open areas with growing shrubs
10	Grasslands	3	Range land
11	Permanent Wetlands	9	Non-forested wetland
12	Croplands	2	Agricultural land
13	Urban and Built-up	1	Urban land
14	Cropland/Natural Vegetatation Mosaic	10	Mixed agricultural and range land
15	Snow and Ice	12	Snow and Ice
16	Barren or Sparsely Vegetated	8	Barren land mostly Desert
17	Water Bodies	7	water, both salt and fresh
	The above 17 entries are identical to previous version of FLEXPART-WRF		
18	Wooded Tundra[1]	6	Mixed Forest including Wetland[2]
19	Mixed Tundra[1]	6+8	50% each
20	Barren Tundra[1]	8	Barren land mostly Desert[2]

[1]Additional classes available in WRF-output files, [2]Adopted from WRF-CHEM.

Table A.2: Conversion table used by FLEXPART-WRF for interpreting USGS land-use in WRF output. The conversion table used by WRF-CHEM is shown for comparison. Dry deposition schemes in WRF-CHEM and FLEXPART-WRF are based on the 11 classes described by Wesely (1989), FLEXPART-WRF also includes a rainforest class described by Jacob & Wofsy (1990).

Index+description	WRF-CHEM[1]	FLEXPART[1]
1 - Urban and built-up land	1	1
2 - Dryland cropland and pasture	2	2
3 - Irrigated cropland and pasture	2	2
4 - Mix. dry/irrg. cropland and pasture	2	2
5 - Cropland/grassland mosaic	2	10
6 - Cropland/woodland mosaic	4	4
7 - Grassland	3	3
8 - Shrubland	3	11
9 - Mixed shrubland/grassland	3	3 and 11[2]
10 - Savanna	3[3]	11
11 - Deciduous broadleaf forest	4	4
12 - Deciduous needleleaf forest	5[4]	4
13 - Evergreen broadleaf forest	4[3]	13[5]
14 - Evergreen needleleaf forest	5	5
15 - Mixed Forest	6	6
16 - Water Bodies	7	7
17 - Herbaceous wetland	9	9
18 - Wooded wetland	6	6
19 - Barren or sparsely vegetated	8	8
20 - Herbaceous Tundra	9	9
21 - Wooded Tundra	6	6
22 - Mixed Tundra	6	6 and 8[2]
23 - Bare Ground Tundra	8	8
24 - Snow or Ice	-[6]	12[6]
25 - No data	8	-

[1]Based on Wesely (1989), [2]FLEXPART-WRF assumes 50% of each class, [3]Always summer, [4]Autumn and winter modified, [5]Based on Jacob & Wofsy (1990), [6]Always winter.

References

Allen, A. G., Mather, T. A., McGonigle, A. J. S., Aiuppa, A., Delmelle, P., Davison, B., Bobrowski, N., Oppenheimer, C., Pyle, D. M., & Inguaggiato, S. (2006). Sources, size distribution, and downwind grounding of aerosols from mount etna. *Journal of Geophysical Research: Atmospheres*, *111*, n/a–n/a. doi:10.1029/2005JD006015. D10302.

Allen, A. G., Oppenheimer, C., Ferm, M., Baxter, P. J., Horrocks, L. A., Galle, B., McGonigle, A. J. S., & Duffell, H. J. (2002). Primary sulfate aerosol and associated emissions from Masaya volcano, Nicaragua. *Journal of Geophysical Research: Atmospheres*, *107*, ACH 5 1–8. doi:10.1029/2002JD002120.

Arellano, S. (2014). *Studies of Volcanic Plumes with Remote Spectroscopic Sensing Techniques – DOAS and FTIR Measurements on Volcanoes of the Network for Observation of Volcanic and Atmospheric Change*. Doktorsavhandlingar vid Chalmers tekniska högskola. Ny serie, no: 3751. Gothenburg: Institutionen för rymd- och geovetenskap, Optisk fjärranalys, Chalmers tekniska högskola.

Baxter, P., Allard, P., Halbwachs, M., Komorowski, J.-C., Woods, A., & Anica, A. (2003). Human health and vulnerability in the Nyiragongo volcano crisis at Goma, Democratic Republic of Congo. *Acta Vulcanologica*, *14*, 109–114.

Brioude, J., Arnold, D., Stohl, A., Cassiani, M., Morton, D., Seibert, P., Angevine, W., Evan, S., Dingwell, A., Fast, J. D., Easter, R. C., Pisso, I., Burkhart, J., & Wotawa, G. (2013). The Lagrangian particle dispersion model FLEXPART-WRF version 3.1. *Geoscientific Model Development*, *6*, 1889–1904. doi:10.5194/gmd-6-1889-2013.

Calabrese, S., Scaglione, S., Milazzo, S., D'Alessandro, W., Bobrowski, N., Giuffrida, G. B., Tedesco, D., Parello, F., & Yalire, M. (2015). Passive degassing at Nyiragongo (D.R. Congo) and Etna (Italy) volcanoes. *Annals of Geophysics*, *57*.

Cuoco, E., Spagnuolo, A., Balagizi, C., Francesco, S. D., Tassi, F., Vaselli, O., & Tedesco, D. (2013a). Impact of volcanic emissions on rainwater chemistry: The case of Mt. Nyiragongo in the Virunga volcanic region (DRC). *Journal of Geochemical Exploration*, *125*, 69–79. doi:10.1016/j.gexplo.2012.11.008.

Cuoco, E., Tedesco, D., Poreda, R. J., Williams, J. C., Francesco, S. D., Balagizi, C., & Darrah, T. H. (2013b). Impact of volcanic plume emissions on rain water chemistry during the January 2010 Nyamuragira eruptive event: Implications for essential potable water resources. *Journal of Hazardous Materials*, *244-245*, 570–581. doi:http://dx.doi.org/10.1016/j.jhazmat.2012.10.055.

Dingwell, A., & Rutgersson, A. (2014). Estimating volcanic ash hazard in European airspace. *Journal of Volcanology and Geothermal Research*, *286*, 55–66. doi:10.1016/j.jvolgeores.2014.08.022.

Galle, B., Johansson, M., Rivera, C., Zhang, Y., Kihlman, M., Kern, C., Lehmann, T., Platt, U., Arellano, S., & Hidalgo, S. (2010). Network for Observation of Volcanic and Atmospheric Change (NOVAC)–A global network for volcanic gas monitoring: Network layout and instrument description. *Journal of Geophysical Research (Atmospheres)*, *115*, D5304. doi:10.1029/2009JD011823.

Gentner, D. R., Ford, T. B., Guha, A., Boulanger, K.,

Brioude, J., Angevine, W. M., de Gouw, J. A., Warneke, C., Gilman, J. B., Ryerson, T. B., Peischl, J., Meinardi, S., Blake, D. R., Atlas, E., Lonneman, W. A., Kleindienst, T. E., Beaver, M. R., Clair, J. M. S., Wennberg, P. O., VandenBoer, T. C., Markovic, M. Z., Murphy, J. G., Harley, R. A., & Goldstein, A. H. (2014). Emissions of organic carbon and methane from petroleum and dairy operations in California's San Joaquin Valley. *Atmospheric Chemistry and Physics*, *14*, 4955–4978. doi:10.5194/acp-14-4955-2014.

Hong, S.-Y., Dudhia, J., & Chen, S.-H. (2004). A Revised Approach to Ice Microphysical Processes for the Bulk Parameterization of Clouds and Precipitation. *Monthly Weather Review*, *132*, 103. doi:10.1175/1520-0493(2004)132<0103:ARATIM>2.0.CO;2.

Jacob, D. J., & Wofsy, S. C. (1990). Budgets of reactive nitrogen, hydrocarbons, and ozone over the Amazon forest during the wet season. *Journal of Geophysical Research: Atmospheres*, *95*, 16737–16754. doi:10.1029/JD095iD10p16737.

Janjić, Z. I. (1994). The step-mountain eta coordinate model: Further developments of the convection, viscous sublayer, and turbulence closure schemes. *Monthly Weather Review*, *122*, 927–945. doi:10.1175/1520-0493(1994)122\%3C0927:TSMECM\%3E2.0.CO;2.

Kain, J. S. (2004). The Kain–Fritsch convective parameterization: An update. *Journal of Applied Meteorology*, *43*, 170–181. doi:10.1175/1520-0450(2004)043<0170:TKCPAU>2.0.CO;2.

Komorowski, J.-C., Tedesco, D., Kasereka, M., Allard, P., Papale, P., Vaselli, O., Durieux, J., Baxter, P., Halbwachs, M., Akumbe, M., Baluku, B., Briole, P., Ciraba, M., Dupin, J.-C., Etoy, O., Garcin, D., Hamaguchi, H., Houlié, N., Kavotha, K. S., Lemarchand, A., Lockwood, J., Lukaya, N., Mavonga, G., de Michele, M., Mpore, S., Mukambilwa, K., Munyololo, F., Newhall, C., Ruch, J., Yalire, M., & Wafula, M. (2003). The January 2002 flank eruption of Nyiragongo volcano (Democratic Republic of Congo): Chronology, evidence for a tectonic rift trigger, and impact of lava flows on the city of Goma. *Acta Vulcanologica*, *15*, 27–62.

Liu, D., Quennehen, B., Darbyshire, E., Allan, J. D., Williams, P. I., Taylor, J. W., Bauguitte, S. J.-B., Flynn, M. J., Lowe, D., Gallagher, M. W., Bower, K. N., Choularton, T. W., & Coe, H. (2015). The importance of Asia as a source of black carbon to the European Arctic during springtime 2013. *Atmospheric Chemistry and Physics*, *15*, 11537–11555. doi:10.5194/acp-15-11537-2015.

Mather, T. A., Allen, A. G., Oppenheimer, C., Pyle, D. M., & McGonigle, A. J. S. (2003). Size-resolved characterisation of soluble ions in the particles in the tropospheric plume of Masaya volcano, Nicaragua: origins and plume processing. *Journal of Atmospheric Chemistry*, *46*, 207–237. doi:10.1023/A:1026327502060.

Platt, U., & Stutz, J. (2008). *Differential Optical Absorption Spectroscopy*. Physics of Earth and Space Environments. Berlin Heidelberg: Springer.

Pohl, B., Crétat, J., & Camberlin, P. (2011). Testing WRF capability in simulating the atmospheric water cycle over Equatorial East Africa. *Climate Dynamics*, *37*, 1357–1379. doi:10.1007/s00382-011-1024-2.

Radke, L. F., Hobbs, P. V., & Stith, J. L. (1976). Airborne measurements of gases and aerosols from volcanic vents on Mt. Baker. *Geophysical Research Letters*, *3*, 93–96. doi:10.1029/GL003i002p00093.

16

Rögnvaldsson, O., Bao, J.-W., Áugústsson, H., & Ólafsson, H. (2008). Downslope windstorm in Iceland – WRF/MM5 model comparison. *Atmos. Chem. Phys.*, *8*, 6437–6468.

Sawyer, G. M., Carn, S. A., Tsanev, V. I., Oppenheimer, C., & Burton, M. (2008). Investigation into magma degassing at Nyiragongo volcano, Democratic Republic of the Congo. *Geochemistry, Geophysics, Geosystems*, *9*, 1–17. doi:`10.1029/2007GC001829`.

Srinivas, C. V., Rakesh, P. T., Hari Prasad, K. B. R. R., Venkatesan, R., Baskaran, R., & Venkatraman, B. (2014). Assessment of atmospheric dispersion and radiological impact from the Fukushima accident in a 40-km range using a simulation approach. *Air Quality, Atmosphere & Health*, *7*, 209–227. doi:`10.1007/s11869-014-0241-3`.

Steensen, T., Stuefer, M., Webley, P., Grell, G., & Freitas, S. (2013). Qualitative comparison of Mount Redoubt 2009 volcanic clouds using the PUFF and WRF-Chem dispersion models and satellite remote sensing data. *Journal of Volcanology and Geothermal Research*, *259*, 235 – 247. doi:`10.1016/j.jvolgeores.2012.02.018`. The 2009 Eruption of Redoubt Volcano, Alaska.

Tedesco, D., Vaselli, O., Papale, P., Carn, S. A., Voltaggio, M., Sawyer, G. M., Durieux, J., Kasereka, M., & Tassi, F. (2007). January 2002 volcano-tectonic eruption of Nyiragongo volcano, Democratic Republic of Congo. *Journal of Geophysical Research: Solid Earth*, *112*. doi:`10.1029/2006JB004762`.

Tewari, M., Chen, F., Wang, W., Dudhia, J., LeMone, M., Mitchell, K., Ek, M., Gayno, G., Wegiel, J., & Cuenca, R. (2004). Implementation and verification of the unified noah land surface model in the wrf model. In *20th conference on weather analysis and forecasting/16th conference on numerical weather prediction* (pp. 11–15).

Wesely, M. (1989). Parameterization of surface resistances to gaseous dry deposition in regional-scale numerical models. *Atmospheric Environment (1967)*, *23*, 1293–1304. doi:`http://dx.doi.org/10.1016/0004-6981(89)90153-4`.

WHO (2000). *Air quality guidelines: classical pollutants*. (2nd ed.). World Health Organization.

WHO (2006). *Air quality guidelines: global update 2005: particulate matter, ozone, nitrogen dioxide, and sulfur dioxide*. (3rd ed.). World Health Organization.

17